Formation of Deformation-Induced Products in a Metastable-β Titanium Alloy during High Temperature Compression

Alireza Samiee [1,*], Gilberto Casillas [2], Mansur Ahmed [1,3], Dmytro G. Savvakin [4], Ryan Naseri [1,2] and Elena Pereloma [1,2]

[1] School of Mechanical, Materials, Mechatronic and Biomedical Engineering, University of Wollongong, Wollongong, NSW 2522, Australia; ma960@uowmail.edu.au (M.A.); pszn725@uowmail.edu.au (R.N.); elenap@uow.edu.au (E.P.)

[2] Electron Microscopy Centre, University of Wollongong, Wollongong, NSW 2519, Australia; gilberto@uow.edu.au

[3] Department of Mechanical Engineering, Kyushu University, Fukuoka 819-0395, Japan

[4] Institute for Metal Physics, National Academy of Sciences of Ukraine, UA-03142 Kiev, Ukraine; savva@imp.kiev.ua

* Correspondence: as097@uowmail.edu.au; Tel.: +61-2-4221-5507

Abstract: A metastable-β titanium alloy, Ti-10V-3Fe-3Al (wt. %), was subjected to thermo-mechanical processing including the compression test at 725 °C, which is below the β transus temperature (780 °C), and at strain rate of 10^{-3} s^{-1}. The presence of phases was determined using transmission electron microscopy and X-ray diffraction. Although the dynamic recovery took place together with slip, both deformation-induced α″ martensite and ω were detected as other operating mechanisms for the first time in metastable-β titanium alloy deformed in α + β region. The volume fraction of stress-induced α″ was higher than that of the same alloy deformed at room temperature due to a higher strain applied. Stress-induced twinning was not operational, which could be related to the priority of slip mechanism at high temperature resulted from thermally-assisted nucleation and lateral migration of kink-pairs.

Keywords: metastable-β titanum alloy; high temperature deformation; stress-induced ω; stress-induced α″martensite; transmission electron microscopy; slip; X-ray diffraction

1. Introduction

Owing to the fact that metastable-β titanium alloys have shown excellent mechanical properties such as high strength to weight ratio, a good merger of toughness and fatigue resistance [1,2], they are widely used in aerospace industry, such as landing gear, air frame and thick section parts which should be forged for the application [3–5].

Production of thick section parts from metastable-β titanium alloys is one of the main challenges of the aerospace industry [3]. Near-net-shape hot forging is an economic manufacturing method for producing large components which results in coveted mechanical properties [6]. Nonetheless, metastable-β titanium alloys, such as Ti-10V-2Fe-3Al (wt. %) (hereafter designed as Ti-10-2-3) utilised in landing gear of Boeing 777, are generally easily affected by small variation in both temperature and strain rate [7]. Therefore, studies have been focused on the hot deformation mechanisms and microstructural evolution under different deformation conditions in order to optimise processing parameters and mechanical properties of metastable-β titanium alloys [8–12].

The studies have shown that the main hot deformation mechanisms in Ti-10-2-3 deformed at above β transus temperature and strain rates from 0.001 to 10 s^{-1} are both dynamic recovery (DRV)

and dynamic recrystallisation (DRX) [13–16]. Akanuma et al. [17] studied the effect of hot deformation on athermal α'' formation for Ti-10-2-3 alloy. After hot compression at 900 °C and 1000 °C, and at strain rates exceeding 0.1 s^{-1}, athermal α'' martensite appeared in the microstructure of the alloy. The contribution of the dislocation stored energy to the chemical potential gave rise to the transformation of β matrix to the athermal α''. Lei et al. [11] similarly concluded that the higher the mechanical instability of β phase that resulted from the deformation above β transus temperature, the more athermal α'' martensite forms. However, limited studies have been conducted on hot deformation of metastable titanium alloys below the β transus temperature. Balasubrahmanyam and Prasad [16] reported that the stress-strain curves of Ti-10-2-3 with fine duplex $\alpha + \beta$ microstructure at temperature lower than β transus temperature and low strain rates (10^{-3} s^{-1}) exhibited steady state behaviour, while at higher strain rate (10 and 100 s^{-1}) the alloy exhibited continuous flow softening behaviour. Jackson et al. [7] revealed that at forging temperature of 750 °C, dynamic recrystallisation is the main process in Ti-10-2-3 with coarse β grains containing a large amount of Widmanstätten α plates.

In the last decade attention has been focused on the formation and operation of both twinning and phase transformation mechanisms including stress-induced α'' martensite and stress-induced ω during deformation of metastable-β titanium alloys at room temperature, such as Ti-10-2-3 [18,19], Ti-10V-3Fe-3Al-0.27O (wt. %) [20], Ti-8.0Mo-3.9Nb-2.0V-3.1Al (wt. %) [21], β-Cez alloy [22] and Ti-12 Mo (wt. %) [23,24]. Depending on the beta phase stability and stress conditions (strain rate, strain path, etc.), the operation of $\{332\}\langle113\rangle_\beta$ and $\{112\}\langle111\rangle_\beta$ twinning systems and/or phase transformations of $\beta \rightarrow \alpha''$ martensite and $\beta \rightarrow \omega$ phase could be activated. The majority of research on transformation-induced plasticity and twinning-induced plasticity in metastable-β titanium alloys was carried out at room temperature. Only a limited amount of mechanical testing was conducted at elevated temperatures. Duerig et al. [19] have shown that with decreasing the tensile test temperature from 250 °C to 20 °C, the triggering stress required to initiate α'' martensite formation in Ti-10-2-3 alloy was continuously decreasing in correlation with the beta phase stability decrease followed by a sharp increase at the temperature below 20 °C.

In this study, a metastable-β Ti-10V-3Fe-3Al (wt. %) alloy (Ti-10-3-3), produced by the cost-effective blended elemental powder metallurgy technique, as described in [25], is investigated after hot deformation at the temperature below the β transus temperature (753 °C $\leq T_\beta \leq$ 806 °C [26]) and at low strain rate followed by water quenching. Owing to the fact that Fe has the fastest diffusivity among the elements used in Ti-10-3-3, and thus improves the powder compact density during sintering [25], the percentage of Fe in the studied alloy is intentionally increased by 1 wt. %. This leads to the increased β phase stability due to increased Mo equivalent [27], which can affect the formation of stress-induced products. V is the main alloying element in the studied alloy and binary Ti-V alloys exhibit isomorphous-type phase diagram [27]. Accordingly, the studied alloy is likely a β-isomorphous alloy due to high V content. Depending on the processing schedule, this alloy could have at ambient temperature either a fully β microstructure on fast cooling from β phase region or $\alpha + \beta$ phases following a slow cooling or holding below the β transus temperature. This study reports on the concurrent formation of deformation-induced α'' martensite and ω, and discusses the reason for this.

2. Materials and Methods

Vacuum arc remelting was used for producing the master alloy whose chemical composition is Ti-62.5V-18.75Fe-18.75Al (wt. %) after which the produced master alloy was milled to reach the powder with less than 40 μm particle size. Then the master alloy in powder state was blended with base titanium powder which had fine particle size (r < 100 μm) and contained 3.5 wt. % hydrogen to produce Ti-10-3-3 alloy. In the next step, the powders were die-pressed under 640 MPa pressure at room temperature to make the green compact with $10 \times 10 \times 70$ mm^3 dimensions. The green compact was sintered under vacuum for four hours at 1250 °C. At the end of this process, the samples were cooled down in the furnace.

After sintering, 10 mm in length by 8 mm in diameter samples were machined and thermo-mechanically processed using a 3500 Gleeble thermo-mechanical simulator (DSI, Poestenkill, USA). In the first, the samples were heated at 10 °C s^{-1} to 900 °C, held for 120 s, then cooled down to 850 °C at 20 °C s^{-1} where 25% reduction in length was applied to reduce the porosity. Then, the samples were cooled at 20 °C s^{-1} to 725 °C and held for 600 s to form α phase. Finally, the samples were compressed at a constant rate of 10^{-3} s^{-1} to 60% length reduction and immediately water quenched to room temperature (Figure 1).
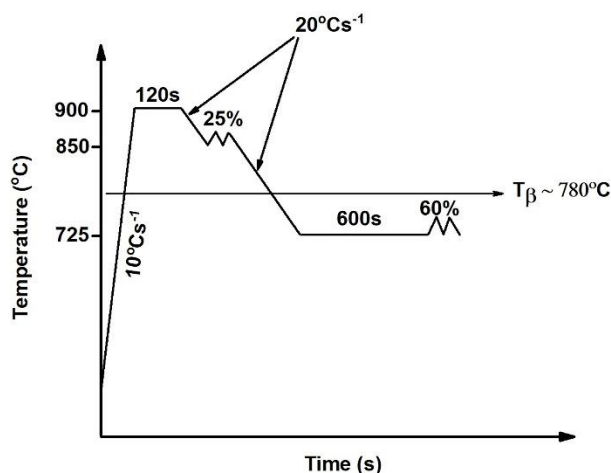

Figure 1. A schematic diagram of the thermo-mechanical processing used in this study.

Microstructure observation was performed at the centre of the sample cross-section ((Normal Direction (ND)) × (Compression Direction (CD) plane)) using a JEOL-JSM 7001F Field Emission Gun-Scanning Electron Microscope (FEG-SEM) (JEOL, Tokyo, Japan)operating at 15 kV voltage and 10 mm working distance. Thin 0.3 mm slices were cut perpendicular to the compression direction using electric discharge machine. They were mechanically thinned down to ~0.12 mm thickness. 3 mm diameter discs were punched out. By using twin jet electropolishing method with an electrolyte containing 5–7% of perchloric acid and methanol, thin foils for transmission electron microscopy (TEM) were prepared at −40 °C. TEM was performed on a probe-corrected scanning transmission electron microscope JEOL ARM200F (JEOL, Tokyo, Japan) operated at 200 kV, equipped with a cold field emission gun.

To identify the present phases, a PANalytical X'Pert PRO Multipurpose diffractometer (MPD) (PANanalytical, Almelo, The Netherlands) with Cu Kα radiation (λ = 0.154 nm) filtered with Ni-monochromator was used. The diffraction pattern from a disc sample (~14 mm diameter and 3 mm thickness) was obtained over the 2θ range of 30–90° under a continuous scanning mode. The step size and the acquisition time were 0.01° and 490 s, respectively. The XRD profile was used to calculate the volume fraction of phases by means of direct comparison method [28].

3. Results

The response of compression test at 725 °C (below the β transus temperature of ~780 °C) and at strain rate of 10^{-3} s^{-1} is shown in Figure 2. A typical true stress-true strain curve shows continuous flow softening after rapid increase up to a maximum stress of ~150 ± 0.4 MPa at 0.07 strain, which is usual response for β titanium alloys deformed at a temperature slightly below β transus (nearly 100 °C) [6,11,29,30]. Although flow softening has been reported for Ti-10-2-3 alloy deformed above the β transus temperature [11,13], the tendency of β titanium alloys deformed below the transus temperature towards flow softening is stronger [11,30].
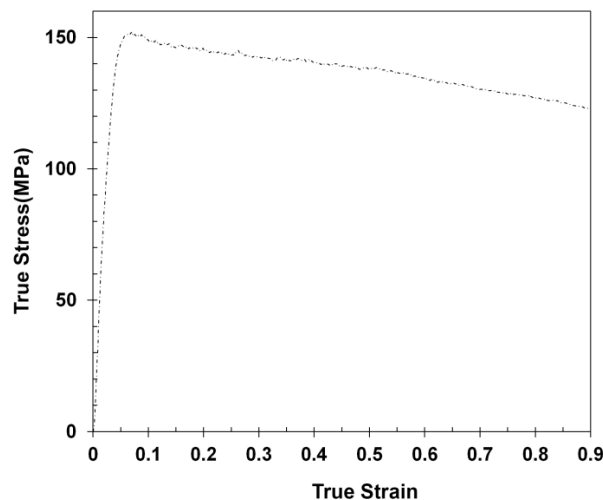
Figure 2. Stress-strain curve for Ti-10-3-3 alloy deformed at 725 °C.

The continuous and uniform reduction of stress flow after the maximum value of the stress demonstrates that the effect of softening was higher than that of hardening. Hot deformed alloys are usually softened by dynamic recovery (DRV) and/or by dynamic recrystallization (DRX). During the former, the dislocations formed during deformation are easily annihilated and readily rearranged as arrays, leading to the formation of subgrains with low angle boundaries, whereas new strain-free grains are formed during DRX [24]. It has been reported that since at low strain rate, such as 10^{-3} s^{-1}, the time required for DRV and DRX is adequate, the softening mechanism is predominant [11].

The microstructure consists of elongated β grains decorated with α formed during 600 s holding at 725 °C before deformation (Figure 3). Some of these grain boundary α precipitates are fragmented as a result of deformation, and finer intergranular α is also present.
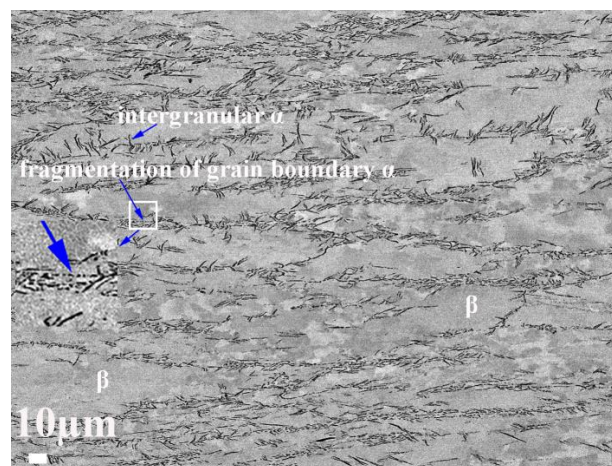

Figure 3. Secondary electron FE-SEM image showing a general view of the microstructure.

Due to the breaking up the lamellar α acting as barriers to the dislocations, flow softening occurs in Ti alloys [31,32]. Fine scale bright contrast β subgrains within elongated ones are also visible in Figure 3. Similar formation of equiaxed β subgrains of ~5 µm size was reported after compression deformation of 1023 alloy at 760 °C and 10^{-2} s^{-1} strain rate [31].

The XRD profile (Figure 4) shows the presence of β, α, ω and α″ peaks. The volume fractions of β, α, ω and α″ were calculated to be 0.760, 0.107, 0.056 and 0.073, respectively.
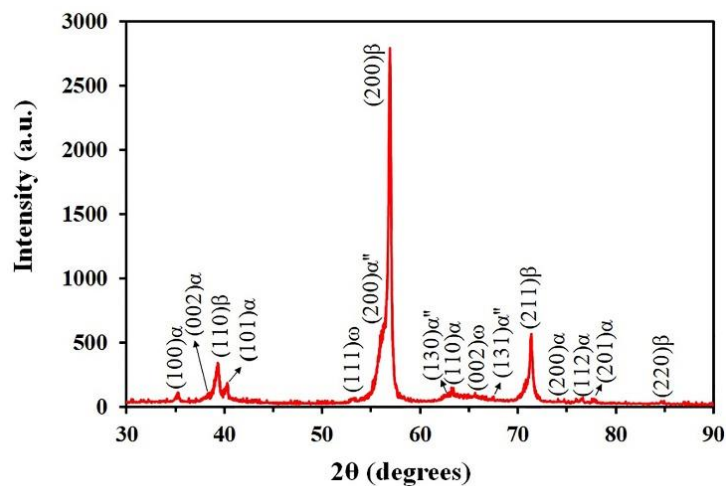
Figure 4. XRD profile obtained from Ti-10-3-3 alloy deformed at 725 °C followed by water quenching to room temperature.

The lattice parameters of the β matrix (*a* = 0.328nm, body centred cubic, bcc), α precipitates (hexagonal close packed, *a* = 0.295 nm, *c* = 0.468 nm), ω phase (hexagonal close packed, *a* = 0.287 nm, *c* = 0.425 nm) and α″ (orthorhombic, *a* = 0.326 nm, *b* = 0.499 nm, *c* = 0.392 nm) calculated from XRD results, are in good agreement with those reported in the literature [27–29].

As a result of heavy deformation (60% reduction in the length of the sample) at 725 °C, coarse slip bands, which are one of the forms of localized deformation [33], were produced in the β matrix (Figure 5a). To the best of our knowledge, we report for the first time the formation of stress-induced α″ (Figure 5b) and stress-induced ω (Figure 5c) during hot deformation in β + α region. The inset in Figure 5b depicts a selected area diffraction pattern (SADP) along the $[\bar{1}13]_\beta$ zone axis. $(\bar{1}10)$ spot of stress-induced α″ appear near to that from $(\bar{1}10)$ of β. The orientation relationship between α″ martensite and β matrix follow the typical relationship, $(\bar{1}\bar{1}0)_\beta \| (\bar{1}\bar{1}0)_\alpha$ and $[\bar{1}13]_\beta \| [002]_{\alpha''}$ [34,35]. Thin lamellar-like morphology of stress-induced ω is depicted in Figure 5c. Figure 5d is a dark field (DF) image showing the presence of athermal ω (ω_{ath}) with ellipsoidal/spherical morphology, which presumably formed on cooling to room temperature of the deformed sample. The SADP shown in the (inset of Figure 5d) demonstrates the sharp β reflections which are consistent with a bcc structure, and the faint reflections at 1/3 and 2/3 $\{112\}_\beta$ positions which are features of ω_{ath} [36]. Both types of ω (insets in Figure 5c,d) illustrate the typical $(111)_\beta // (0001)_\omega$ and $[0\bar{1}1]_\beta // [11\bar{2}0]_\omega$ orientation relationship with β matrix [37,38].
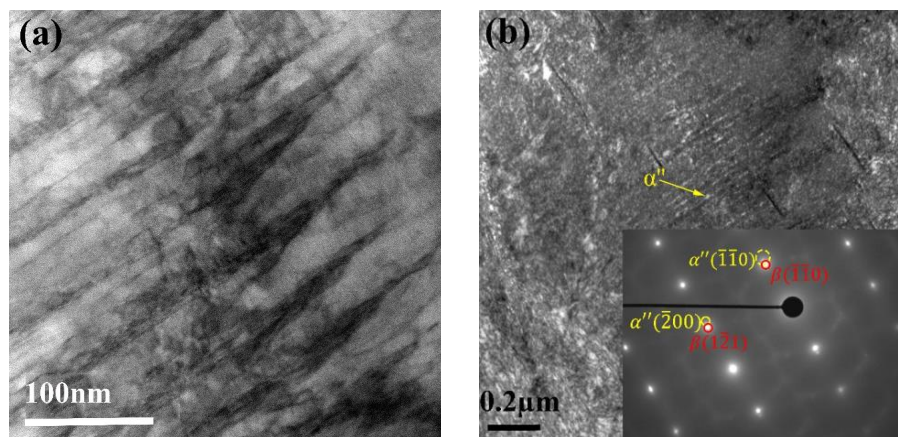

Figure 5. *Cont.*

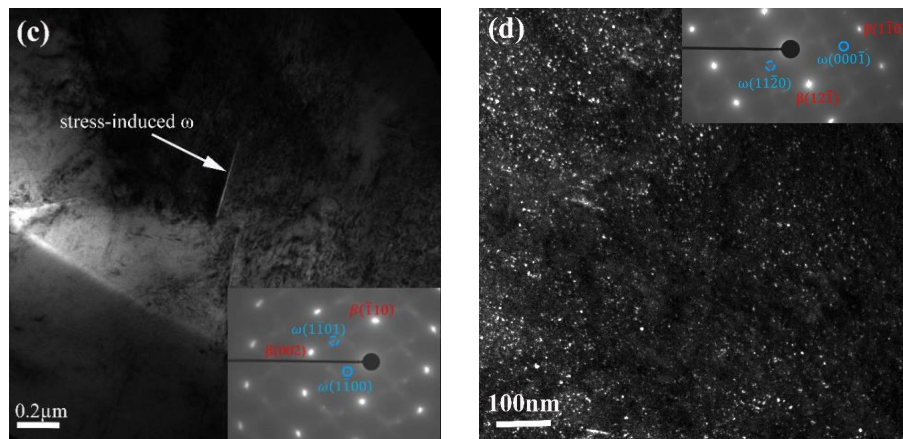**Figure 5.** (**a**) Bright field image revealing continuous slip bands in the β matrix. (**b**) Dark field (DF) image showing the presence of stress-induced α″ martensite obtained using the reflection in dashed yellow circle in the inset (Zone axis: $[\bar{1}13]_\beta \| [002]_{\alpha''}$). (**c**) DF image revealing stress-induced ω taken using the reflection in dashed blue circle in the inset (Zone axis: $[110]_\beta \| [11\bar{2}0]_\omega$). (**d**) DF image displaying ω_{ath} precipitation, which is taken using dashed blue circle in the inset (Zone axis: $[113]_\beta \| [\bar{1}100]_\omega$).

4. Discussion

While the true stress-true strain curve (Figure 2) does not show stress plateau characteristics of the stress-induced α″ formation [19,39], the observed α″ (Figure 5b) can be a stress-induced one for the following reasons. Firstly, it has been revealed for Ti-10-2-3 alloy [7,40] that when the alloy solution treated below β transus temperature and quenched in water or He gas, the athermal α″ was not formed. The main reason is related to the presence of α phase in the β at below the β transus temperature, which decreases the size of metastable β regions, increases the stability of the β phase and inhibits the formation of athermal α″, compared to the Ti-10-2-3 alloy quenched from the above β transus temperature [40]. As a result, due to the deformation temperature utilised in this study (below the β transus temperature), the probability of athermal α″ formation is very low. Secondly, as the foils were electropolished and the observations were carried out in 200–400 nm thick regions, the deformed surfaces formed during the earlier preparation step of fine grinding were removed. Thirdly, the observed morphology of stress-induced ω (Figure 5c) clearly indicates its deformation-induced origin, and points to the possibility that observed α″ martensite is deformation-induced one.

The amount of α″ martensite formed in this study is nearly 2% higher than that formed after room temperature compression to 0.4 strain of the same Ti-10-3-3 alloy quenched from 725 °C [33,34]. This is despite the stability of β matrix deformed at 725 °C (near β transus temperature) being higher than that of β parent at room temperature [41]. This difference can be related to the higher amount of true strain (0.9 compared to 0.4) which has been applied in this study.

Liu et al. [42] proposed the following Equation (1) for the free energy change of $\Delta G^{\beta \to \alpha''}$ (the transformation of β parent to the stress-induced α″):

$$\Delta G^{\beta \to \alpha''} = (\Delta H^{\beta \to \alpha''} - T\Delta S^{\beta \to \alpha''}) + \Delta E_{el} + \delta E_{irr} - \frac{1}{\rho}\sigma\varepsilon_{tr} - (\frac{1}{2\rho})[(\sigma^2/E_{\alpha''}) - (\sigma^2/E_\beta)], \quad (1)$$

where, $\Delta H^{\beta \to \alpha''}$ is the difference in enthalpy, T is the test temperature and $\Delta S^{\beta \to \alpha''}$ represents the change in entropy. $(\Delta H^{\beta \to \alpha''} - T\Delta S^{\beta \to \alpha''})$ is widely introduced as the chemical free energy change during the phase transformation. Owing to the fact that both $\Delta H^{\beta \to \alpha''} < 0$ and $\Delta S^{\beta \to \alpha''} < 0$ [42], increasing the test temperature from room temperature to 725 °C raises the chemical free energy change, so it makes the β → α″ transformation more difficult. Atoms are located at (0,0,0), (a/2,b/2,0), (0,2b/3,c/2), (a/2,b/6,c/2) in orthorhombic stress-induced α″, while the β parent has a bcc

structure [19]. According to the lattice parameters mentioned earlier for β matrix and stress-induced α″, the volume change resulted from transformation of β to stress-induced α″ is nearly 80%, so the internal elastic energy term ΔE_{el} is an important factor and it increases the free energy. The term $\frac{1}{\rho}\sigma\varepsilon_{tr}$ (σ: uniaxial stress, ε_{tr}: transformation strain and ρ: phase density) which is the force-displacement work related to the transformation owing to the lattice distortion of α″, which does not alter notably with temperature. Although both $E_{\alpha''}$ (Young's modulus of stress-induced α″) and E_{β} (Young's modulus of β) decrease with raising the temperature, the elastic term $(1/2\rho)\,[(\sigma^2/E_{\alpha''}) - (\sigma^2/E_{\beta})]$ contributes to the formation of the stress-induced α″ because it has been assumed that $E_{\alpha''}$ is significantly different from E_{β} [43]. Thus, the energy which is released due to the difference in $E_{\alpha''}$ and E_{β} decreases $\Delta G^{\beta \,\rightarrow\, \alpha''}$ and assists in the formation of stress-induced α″. The term δE_{irr} is the irreversible energy required for overcoming the internal friction to phase boundary movement. Furthermore, at high temperature (725 °C) the stability of β matrix is far higher than that of β matrix at the room temperature. Consequently, increasing the temperature of transformation from room temperature to 725 °C raises the amount of δE_{irr} leading to the increase of $\Delta G^{\beta \,\rightarrow\, \alpha''}$. As a result, the transformation of β matrix to stress-induced α″ martensite at 725 °C is more difficult than that of β matrix deformed at room temperature, so the higher amount of deformation (0.9 compared to 0.4) is required at high temperature to obtain a deformation-induced α″.

In this study, two kinds of ω phase were noticed: (1) nanosized spherical or ellipsoidal particles (ω_{ath}) (Figure 5d) that have been observed to occur on accelerated cooling in metastable-β titanium alloys [18,20,38] and (2) lamellae ω (stress-induced ω) (Figure 5c) which has been reported in titanium alloys after plastic deformation [23,44,45]. Shuffle of atoms in $\{112\}_{\beta}$ planes in the direction of $\langle 111 \rangle$ has been suggested as the formation mechanism for both ω types [44]. However, Hsiung et al. [45] reported the glide of partial dislocations of $1/3\langle 111 \rangle$, $1/6\langle 111 \rangle$ and $1/12\langle 111 \rangle$, which are formed from $1/2\langle 111 \rangle$ perfect dislocation, as the formation mechanism of stress-induced ω.

Besides, due to the stability of β matrix at 725 °C, slip of dislocations (Figure 5a) is one of the major deformation mechanisms detected in Ti-10-3-3 alloy, while twinning mechanism reported by Ahmed et al. [18,20] for Ti-10-3-3 deformed at room temperature was not observed. In materials with bcc crystal structures, a/2<111> dislocation is split into three fractional a/6<111> dislocations, which initially glide along their individual $\{112\}_{\beta}$ planes under the resolved shear stress and then cross-slip onto the most stressed $\{112\}_{\beta}$ plane to form a twin nucleus [46,47]. As at low temperatures, the mobility of dislocations is reduced, the twinning is favoured contrarily to the high temperature where the mobility of dislocations is high favouring their slip; which proceeds by the thermally-assisted nucleation and lateral migration of kink-pairs [48,49]. As a result, in this study, the high temperature of deformation can be the main reason of the absence of twinning as the deformation mechanism.

5. Conclusions

To summarise, while the main deformation mechanisms for the Ti-10-3-3 alloy deformed (ε = 0.9) at 725 °C (below β transus temperature of 780 °C) and strain rate of 10^{-3} s^{-1} were DRV and slip, both deformation-induced α″ martensite and ω were detected for the first time in metastable-β titanium alloy deformed in α + β region. Twinning was not observed in this study, which could be associated with the proceeding of slip at high temperature through nucleation and lateral movement of kink-pairs.

Author Contributions: Dmytro G. Savvakin designed the alloy composition and produced the alloy by BEMP. Mansur Ahmed and Elena Pereloma designed the thermo-mechanical processing schedule. Mansur Ahmed conducted Gleeble thermo-mechanical simulation and participated in data discussions. Ryan Naseri carried out XRD test and together with Mansur Ahmed analysed compression test data. All TEM images were taken by Gilberto Casillas, who also contributed to their analysis. Alireza Samiee analysed SEM, XRD and TEM data. He wrote the first draft of the paper and subsequently improved it with the help from Elena Pereloma. Elena Pereloma supervised all stages of this work and participated in data discussion.

Conflicts of Interest: The authors declare no conflict of interest.

References

1. Peters, J.; Lütjering, G.; Nalla, R.; Altenberger, I.; Ritchie, R. High Cycle Fatigue of Beta-Titanium Alloys. In Proceedings of the Eighth International Fatigue Congress, Stockholm, Sweden, 3–7 June 2002.
2. Jha, S.K.; Ravichandran, K.S. High-cycle fatigue resistance in beta-titanium alloys. *JOM* **2000**, *52*, 30–35. [CrossRef]
3. Coakley, J.; Vorontsov, V.A.; Jones, N.G.; Radecka, A.; Bagot, P.A.; Littrell, K.C.; Heenan, R.K.; Hu, F.; Magyar, A.P.; Bell, D.C. Precipitation processes in the Beta-Titanium alloy Ti–5Al–5Mo–5V–3Cr. *J. Alloys Compd.* **2015**, *646*, 946–953. [CrossRef]
4. Kent, D.; Wang, G.; Wang, W.; Dargusch, M. Influence of ageing temperature and heating rate on the properties and microstructure of β Ti alloy, Ti–6Cr–5Mo–5V–4Al. *Mater. Sci. Eng. A* **2012**, *531*, 98–106. [CrossRef]
5. Nag, S.; Banerjee, R.; Srinivasan, R.; Hwang, J.; Harper, M.; Fraser, H. ω-Assisted nucleation and growth of α precipitates in the Ti–5Al–5Mo–5V–3Cr–0.5 Fe β titanium alloy. *Acta Mater.* **2009**, *57*, 2136–2147. [CrossRef]
6. Fan, J.; Kou, H.; Lai, M.-J.; Tang, B.; Chang, H.; Li, J. Characterization of hot deformation behavior of a new near beta titanium alloy: Ti-7333. *Mater. Des.* **2013**, *49*, 945–952. [CrossRef]
7. Jackson, M.; Dashwood, R.; Flower, H.; Christodoulou, L. The microstructural evolution of near beta alloy Ti-10V-2Fe-3Al during subtransus forging. *Metall. Mater. Trans. A* **2005**, *36*, 1317–1327. [CrossRef]
8. Fan, J.; Kou, H.; Lai, M.; Tang, B.; Chang, H.; Li, J. Hot deformation mechanism and microstructure evolution of a new near β titanium alloy. *Mater. Sci. Eng. A* **2013**, *584*, 121–132. [CrossRef]
9. Jones, N.; Jackson, M. On mechanism of flow softening in Ti–5Al–5Mo–5V–3Cr. *Mater. Sci. Technol.* **2011**, *27*, 1025–1032. [CrossRef]
10. Warchomicka, F.; Poletti, C.; Stockinger, M. Study of the hot deformation behaviour in Ti–5Al–5Mo–5V–3Cr–1Zr. *Mater. Sci. Eng. A* **2011**, *528*, 8277–8285. [CrossRef]
11. Lei, L.; Huang, X.; Wang, M.; Wang, L.; Qin, J.; Li, H.; Lu, S. Effect of hot compressive deformation on the martensite transformation of Ti–10V–2Fe–3Al titanium alloy. *Mater. Sci. Eng. A* **2011**, *530*, 591–601. [CrossRef]
12. Jones, N.; Dashwood, R.; Dye, D.; Jackson, M. The flow behavior and microstructural evolution of Ti-5Al-5Mo-5V-3Cr during subtransus isothermal forging. *Metall. Mater. Trans. A* **2009**, *40*, 1944–1954. [CrossRef]
13. Zhao, J.; Zhong, J.; Yan, F.; Chai, F.; Dargusch, M. Deformation behaviour and mechanisms during hot compression at supertransus temperatures in Ti-10V-2Fe-3Al. *J. Alloys Compd.* **2017**, *710*, 616–627. [CrossRef]
14. Furuhara, T.; Poorganji, B.; Abe, H.; Maki, T. Dynamic recovery and recrystallization in titanium alloys by hot deformation. *JOM* **2007**, *59*, 64–67. [CrossRef]
15. Quan, G.-Z.; Lv, W.-Q.; Liang, J.-T.; Pu, S.-A.; Luo, G.-C.; Liu, Q. Evaluation of the hot workability corresponding to complex deformation mechanism evolution for Ti–10V–2Fe–3Al alloy in a wide condition range. *J. Mater. Process. Technol.* **2015**, *221*, 66–79. [CrossRef]
16. Balasubrahmanyam, V.; Prasad, Y. Hot deformation mechanisms in metastable beta titanium alloy Ti–10V–2Fe–3Al. *Mater. Sci. Technol.* **2001**, *17*, 1222–1228. [CrossRef]
17. Akanuma, T.; Matsumoto, H.; Sato, S.; Chiba, A.; Inagaki, I.; Shirai, Y.; Maeda, T. Enhancement of athermal α″ martensitic transformation in Ti–10V–2Fe–3Al alloy due to high-speed hot deformation. *Scr. Mater.* **2012**, *67*, 21–24. [CrossRef]
18. Ahmed, M.; Wexler, D.; Casillas, G.; Ivasishin, O.M.; Pereloma, E.V. The influence of β phase stability on deformation mode and compressive mechanical properties of Ti–10V–3Fe–3Al alloy. *Acta Mater.* **2015**, *84*, 124–135. [CrossRef]
19. Duerig, T.; Albrecht, J.; Richter, D.; Fischer, P. Formation and reversion of stress induced martensite in Ti-10V-2Fe-3Al. *Acta Metall.* **1982**, *30*, 2161–2172. [CrossRef]
20. Ahmed, M.; Wexler, D.; Casillas, G.; Savvakin, D.G.; Pereloma, E.V. Strain rate dependence of deformation-induced transformation and twinning in a metastable titanium alloy. *Acta Mater.* **2016**, *104*, 190–200. [CrossRef]

21. Zhang, L.C.; Zhou, T.; Aindow, M.; Alpay, S.P.; Blackburn, M.J.; Wu, M.H. Nucleation of stress-induced martensites in a Ti/Mo-based alloy. *J. Mater. Sci.* **2005**, *40*, 2833–2836. [CrossRef]

22. Grosdidier, T.; Philippe, M.-J. Deformation induced martensite and superelasticity in a β-metastable titanium alloy. *Mater. Sci. Eng. A* **2000**, *291*, 218–223. [CrossRef]

23. Sun, F.; Zhang, J.; Marteleur, M.; Gloriant, T.; Vermaut, P.; Laillé, D.; Castany, P.; Curfs, C.; Jacques, P.; Prima, F. Investigation of early stage deformation mechanisms in a metastable β titanium alloy showing combined twinning-induced plasticity and transformation-induced plasticity effects. *Acta Mater.* **2013**, *61*, 6406–6417. [CrossRef]

24. Marteleur, M.; Sun, F.; Gloriant, T.; Vermaut, P.; Jacques, P.J.; Prima, F. On the design of new β-metastable titanium alloys with improved work hardening rate thanks to simultaneous TRIP and TWIP effects. *Scr. Mater.* **2012**, *66*, 749–752. [CrossRef]

25. Savvakin, D.G.; Carman, A.; Ivasishin, O.M.; Matviychuk, M.V.; Gazder, A.A.; Pereloma, E.V. Effect of iron content on sintering behavior of Ti-V-Fe-Al near-β titanium alloy. *Metall. Mater. Trans. A* **2012**, *43*, 716–723. [CrossRef]

26. Guo, Z.; Malinov, S.; Sha, W. Modelling beta transus temperature of titanium alloys using artificial neural network. *Comput. Mater. Sci.* **2005**, *32*, 1–12. [CrossRef]

27. Polmear, I. *Light Metals: From Traditional Alloys to Nanocrystals*, 4th ed.; Elsevier's Science and Technology: Oxford, UK, 2006; pp. 299–335.

28. Cullity, B.D.; Stock, S. *Elements of X-ray Diffraction*; Pearson Education Limited: Essex, UK, 2014.

29. Wang, Z.-J.; Qiang, H.-F.; Wang, X.-R.; Guang, W. Constitutive model for a new kind of metastable β titanium alloy during hot deformation. *Trans. Nonferrous Met. Soc. China* **2012**, *22*, 634–641. [CrossRef]

30. Balasubrahmanyam, V.; Prasad, Y. Deformation behaviour of beta titanium alloy Ti–10V–4.5 Fe–1.5 Al in hot upset forging. *Mater. Sci. Eng. A* **2002**, *336*, 150–158. [CrossRef]

31. Jackson, M.; Jones, N.; Dye, D.; Dashwood, R. Effect of initial microstructure on plastic flow behaviour during isothermal forging of Ti–10V–2Fe–3Al. *Mater. Sci. Eng. A* **2009**, *501*, 248–254. [CrossRef]

32. Zhao, J.; Zhong, J.; Zhou, M.; Chai, F.; Yan, F. The effect of alpha phase on flow softening and deformation of Ti–10V–2Fe–3Al. *Mater. Sci. Technol.* **2017**, *33*, 1993–2003. [CrossRef]

33. Warner, C.P. Mechanisms of Strain Localization in Plane Strain Compression of Aluminum and Aluminum Alloys. Ph.D. Thesis, University of Pennsylvania, Philadelphia, PA, USA, 1997. Disertation available from ProQuest AAI9727310.

34. Barriobero-Vila, P.; Requena, G.; Warchomicka, F.; Stark, A.; Schell, N.; Buslaps, T. Phase transformation kinetics during continuous heating of a β-quenched Ti–10V–2Fe–3Al alloy. *J. Mater. Sci.* **2015**, *50*, 1412–1426. [CrossRef]

35. Cai, M.-H.; Lee, C.-Y.; Kang, S.; Lee, Y.-K. Fine-grained structure fabricated by strain-induced martensite and its reverse transformations in a metastable β titanium alloy. *Scr. Mater.* **2011**, *64*, 1098–1101. [CrossRef]

36. De Fontaine, D.; Paton, N.; Williams, J. The omega phase transformation in titanium alloys as an example of displacement controlled reactions. *Acta Metall.* **1971**, *19*, 1153–1162. [CrossRef]

37. Furuhara, T.; Maki, T.; Makino, T. Microstructure control by thermomechanical processing in β-Ti–15–3 alloy. *J. Mater. Process. Technol.* **2001**, *117*, 318–323. [CrossRef]

38. Ahmed, M.; Li, T.; Casillas, G.; Cairney, J.M.; Wexler, D.; Pereloma, E.V. The evolution of microstructure and mechanical properties of Ti–5Al–5Mo–5V–2Cr–1Fe during ageing. *J. Alloys Compd.* **2015**, *629*, 260–273. [CrossRef]

39. Grosdidier, T.; Roubaud, C.; Philippe, M.-J.; Combres, Y. The deformation mechanisms in the β-metastable β-Cez titanium alloy. *Scr. Mater.* **1997**, *36*, 21–28. [CrossRef]

40. Neelakantan, S.; San Martin, D.; Rivera-Diaz-del-Castillo, P.; Van der Zwaag, S. Plasticity induced transformation in a metastable β Ti-1023 alloy by controlled heat treatments. *Mater. Sci. Technol.* **2009**, *25*, 1351–1358. [CrossRef]

41. Joshi, V.A. *Titanium Alloys: An Atlas of Structures and Fracture Features*; Taylor & Francis: Boca Raton, FL, USA, 2006.

42. Liu, Y.; Yang, H. The concern of elasticity in stress-induced martensitic transformation in NiTi. *Mater. Sci. Eng. A* **1999**, *260*, 240–245. [CrossRef]

43. Bhattacharjee, A.; Bhargava, S.; Varma, V.; Kamat, S.; Gogia, A. Effect of β grain size on stress induced martensitic transformation in β solution treated Ti–10V–2Fe–3Al alloy. *Scr. Mater.* **2005**, *53*, 195–200. [CrossRef]

44. Cheng, G.; Yuan, H.; Jian, W.; Xu, W.; Millett, P.; Zhu, Y. Deformation-induced ω phase in nanocrystalline Mo. *Scr. Mater.* **2013**, *68*, 130–133. [CrossRef]

45. Hsiung, L.; Lassila, D. Shock-induced deformation twinning and omega transformation in tantalum and tantalum–tungsten alloys. *Acta Mater.* **2000**, *48*, 4851–4865. [CrossRef]

46. Sleeswyk, A. $\frac{1}{2}$ Screw dislocations and the nucleation of {112} twins in the Bcc Lattice. *Philos. Mag.* **1963**, *8*, 1467–1486. [CrossRef]

47. Lagerlof, K. On deformation twinning in bcc metals. *Acta Metall. Mater.* **1993**, *41*, 2143–2151. [CrossRef]

48. Seeger, A.; Schiller, P. The formation and diffusion of kinks as the fundamental process of dislocation movement in internal friction measurements. *Acta Metall.* **1962**, *10*, 348–357. [CrossRef]

49. Ogawa, K. Edge dislocations dissociated in {112} planes and twinning mechanism of bcc metals. *Philos. Mag.* **1965**, *11*, 217–233. [CrossRef]